First-principles theory of nanoscale pattern formation in ultrathin alloy films: A comparative study of Fe-Ag on Ru(0001) and Mo(110) substrates

Bo Yang,[1,*] Tejodher Muppidi,[2] Vidvuds Ozoliņš,[2] and Mark Asta[1]
[1]*Department of Chemical Engineering and Materials Science, University of California, Davis, California 95616, USA*
[2]*Department of Materials Science and Engineering, University of California, Los Angeles, California 90095, USA*
(Received 2 February 2008; revised manuscript received 8 April 2008; published 8 May 2008)

The formation of nanoscale self-assembled compositional patterns in monolayer bulk-immiscible alloy films is studied from first principles within the framework of a previously proposed hybrid atomistic-continuum model [V. Ozoliņš *et al.*, Phys. Rev. Lett. **88**, 096101 (2002)]. The details surrounding the parametrization of the model from first-principles calculations are described for both hexagonal (0001) and bcc (110) substrates, and we demonstrate how the theoretical model can be employed in Monte Carlo simulations as a predictive framework for modeling the structure and finite-temperature stability of compositional patterns. The methodology is applied in a comparative study of equiatomic FeAg pseudomorphic alloy films on Mo(110) and Ru(0001) substrates. Stripe patterns with periodicities of a few nanometers are predicted to be stable in both systems, which is in good agreement with available experimental data for FeAg/Mo(110). The regularity of the stripe patterns and their stability with respect to disordering are found to be substantially enhanced on the anisotropic Mo(110) substrate relative to the nearly isotropic Ru(0001) surface, despite the slightly stronger ordering energetics in the latter system. A comparison of the results of the present study to the predictions of continuum theories commonly employed to describe pattern formation on crystalline surfaces serves to highlight the limitations of such models in the application to patterns with periodicities with length scales of approximately ten atomic spacings.

DOI: 10.1103/PhysRevB.77.205408 PACS number(s): 68.35.Md, 68.35.Dv, 68.55.Nq

I. INTRODUCTION

Nanoscale materials hold promise for many novel applications ranging from single electron transistors[1] to molecular electronics,[2] quantum dot lasers,[3] and quantum computing.[4] Obtaining large ordered arrays of nearly identical nanostructures has been long recognized as one of the central challenges to the widespread adoption of these new technologies. For instance, enormous effort has been devoted to studying self-assembled quantum dots[5] (SAQDs) obtained during the Stranski–Krastanov epitaxial growth mode,[6] but the disorder in the sizes and spatial distribution of SAQDs have been difficult to control due to the random nature of their nucleation. There is a growing consensus that "directed self-assembly," where an externally imposed pattern serves as a mask, nudging atoms and molecules toward predefined spatial locations, might offer the solution to these difficulties if one can devise efficient methods of obtaining patterned masks or creating external fields with nanometer-scale periodicities.

Ordered patterns with linear dimensions between a few and a few hundred nanometers, such as those shown in Fig. 1, have been observed in several low-dimensional systems:[7] Langmuir–Blodgett monolayers,[8] diblock copolymers,[9] magnetic films,[10] fluids,[11] and surfaces.[12–21] In addition to being fundamentally interesting, these patterns may also be transferred to semiconductor surfaces and used for directed self-assembly.[22] In this paper, we will be concerned with the phenomenon of pattern formation in flat ultrathin films composed of bulk-immiscible elements. Several such systems have been studied in recent experiments,[23–27] and the term "self-assembled lateral multilayers" has been used to refer to the resulting stripe phases.[24] We will show how to construct quantitative first-principles models of the thermodynamics of nanoscale compositional ordering based on the accurate and parameter-free density-functional theory (DFT) method of total energy calculations. These models can be used to study the structure, thermal stability, and phase transitions in monolayer alloy films, as well as to search for new surface alloy systems that form robust self-assembled patterns with nanometer-scale periodicities.

This paper is organized as follows. Section II reviews the current understanding in the field and describes the physical and mathematical bases of our model. Section III describes an application of this formalism to equiatomic Co-Ag and Fe-Ag alloys on two substrates commonly employed in experimental studies of magnetic alloy thin films, namely, the isotropic Ru(0001) and anisotropic Mo(110) surfaces; a comparison of results on these two substrates highlights the nature of the effects of the substrate on the process of pattern formation. The results of the study are presented in Sec. IV,

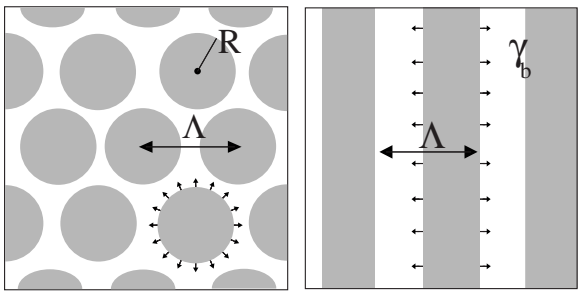

FIG. 1. Ordered surface patterns forming due to competition between short-range attractive and long-range repulsive forces. The arrows denote elastic relaxations due to size mismatch between the alloy constituents.

and these results are discussed in light of experimental observations and previous theoretical studies in Sec. V, which also outlines directions for future research. The main conclusions are summarized in Sec. VI.

II. MODEL FOR ALLOY-FILM ENERGETICS

This section begins with a short review of the current understanding of pattern formation in surface alloy films. We then review the harmonic formalism proposed by Ozoliņš *et al.*[28] for modeling the competing elastic and chemical contributions underlying the configurational energetics of pseudomorphic monolayer alloy films. Subsequently, we give the details of the model parametrization for Fe-Ag films on Ru(0001) and Mo(110) by using elastic continuum Green's functions for the substrate response.

A. Theoretical background

It is well understood that regular patterns (see Fig. 1) can form due to thermodynamic ordering tendencies arising from competing interactions that favor like neighbors (phase separation) on short distances and unlike neighbors (intermixing) on long distances.[7] In a simple Ising-like lattice model, ordering tendencies between the nearest neighbors (NNs) are governed by an effective-pair interaction:

$$J_{\mathrm{NN}} = \frac{1}{4}(V_{AA} + V_{BB} - 2V_{AB}), \tag{1}$$

where V_{AA}, V_{BB}, and V_{AB} are the configurationally averaged energies of *A*-*A*, *B*-*B*, and *A*-*B* bonds, respectively. Pattern-forming systems favor like-atom NN bonds, $J_{\mathrm{NN}}<0$. For instance, in the case of a surface alloy formed by immiscible species, such as Fe and Ag (Ref. 24) or Co and Ag,[25] Fe-Ag and Co-Ag bonds are energetically costly in comparison with like-neighbor (Fe-Fe, Co-Co, and Ag-Ag) bonds. Thus, the nearest-neighbor energy is minimized in a phase-segregated state with large patches of Co or Fe and Ag. However, the size mismatch between the surface species and the substrate imposes a high energetic penalty on the phase-segregated state due to epitaxial strain. As a compromise, the system forms patterns, which allow for a partial relief of the surface stress (indicated by the arrows in Fig. 1) at the expense of introducing line boundaries between the two phases. Quite generally, bulk immiscibility and atomic size mismatch are characteristic features of binary alloys that form surface patterns.[29]

A quantitative continuum theory for pattern formation on surfaces was developed by Marchenko.[30] Within this isotropic continuum theory of elastic relaxations, the formation of surface patterns occurs due to the existence of surface stress differences between two coexisting phases (gray and white in Fig. 1). The continuum elasticity theory predicts that the reduction in energy due to the relaxation of the surface stress is sufficient to overcome the positive boundary energy associated with the line interface between the two phases, $E_b = \gamma_b \int dl$ (where $\gamma_b > 0$). Indeed, in periodic striped phases, the elastic relaxation energy exhibits a logarithmic dependence on the period Λ:

$$\Delta E_{\mathrm{el}} = -\frac{(\sigma_A - \sigma_B)^2(1-\nu^2)}{\pi E} \ln\frac{\Lambda}{b}, \tag{2}$$

where σ_A and σ_B are the surface stresses of the two phases, ν and E are the Poisson ratio and Young's modulus of the substrate, and b is a system-specific length scale below which the continuum elasticity theory does not hold and an atomistic description is required; this parameter is typically a few interatomic spacings in magnitude. Equation (2) shows that for sufficiently large periods Λ, the elastic relaxation energy will always overcome the energy cost of introducing line interfaces between the surface phases. The ground-state properties of this model were studied by Ng and Vanderbilt,[31] who found that the periodic patterns shown in Fig. 1 are the stable ground states on an isotropic surface, with stripes being stable near the 50-50 composition and disks (inverted disks) being favored for *A*-rich (*B*-rich) compositions.

Microscopic effects and thermal fluctuations have been extensively studied by Singer and co-workers,[32–35] who considered a spin-$\frac{1}{2}$ lattice model with nearest-neighbor interactions of ferromagnetic type ($J_{\mathrm{NN}}<0$) and weaker long-ranged interactions of antiferromagnetic type, $V(r)=\frac{g\theta(r)}{r^3}$, where r is the separation between sites, g is the strength of the interaction, and $\theta(r)$ is a smooth cutoff function that obeys $\lim_{r\to\infty}\theta(r)=1$ and cancels the $1/r^3$ divergence as $r\to 0$. Near the equiatomic composition, these authors found that the ordered stripe phase disorders (melts) via a continuous defect-mediated phase transition of the Kosterlitz–Thouless (KT) type.[36–39] The transition temperature is found to increase with decreasing ratio, $\eta=|g/J_{\mathrm{NN}}|$, approaching the two-dimensional (2D) Ising value with Ising-like disordering within the stripes in the limit of small η, corresponding to higher values of stripe width Λ. For applications to pattern formation in alloy films, the discrete lattice model considered by Singer and co-workers correctly captures the dipolar nature of the strain-induced interactions at large distances, as predicted by the Marchenko[30] theory (e.g., Ref. 31), and the competing effects of chemistry (through J_{NN}) at short distances; however, the application of the model to specific alloys is complicated by the fact that the functional form of $\theta(r)$ is, in general, unknown for realistic systems.

In Ref. 28, we developed a relatively simple, yet versatile model of surface alloys, which gives an explicit functional form for the interatomic interactions and a recipe to determine them from *ab initio* calculations, allowing for direct contact with experimental results in specific systems. Analytical expressions for elastic relaxation energies and the associated displacement fields were derived in the limits of "stiff" and "soft" substrates. In the stiff-substrate limit, which is found to be appropriate for describing the systems of interest here, it is assumed that the displacements in the substrate, which are induced by the epitaxial film, are small in magnitude relative to those within the alloy layer. In this case, the elastic energy in the film can be described within a harmonic limit of the well-known Frenkel–Kontorova model,[40] while the energy associated with substrate deformation is calculated by using continuum expressions[30,41,42] for the reduction in elastic energy associated with the relaxation

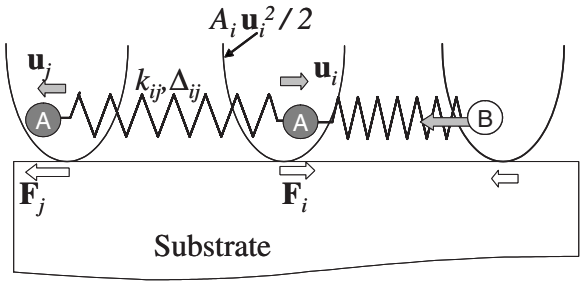

FIG. 2. Schematic model for the energetics of a pseudomorphic alloy film.

of the surface force distributions imposed by the alloy-film displacements.

We will show that in many cases of practical interest,[24,25,43,44] the Marchenko[30] theory does not provide an accurate description of the energetics of thin-film alloy systems because the periodicity of the stable stripes is well below the limit where the substrate-mediated contribution to the elastic displacement field dominates. Instead, the elastic relaxation energy is determined almost entirely by displacements within the surface layer. At intermediate length scales, elastic interactions exponentially[28] decay and display the asymptotic $1/r^3$ dipolar form, which is predicted by the Marchenko[30] theory, only after approximately 15–20 lattice parameters. The model presented below fills the gap between the cases of short-period ordering described by conventional alloy theoretical methods based on short-range Ising models, such as that for Pd-Au/Ru(0001),[45] and long-wavelength modulated phases that are accurately described by the continuum theory of Ng and Vanderbilt[31] and by the scaling theory of Stoycheva and Singer.[33,34] Importantly, our work can be used to provide *ab initio*-based quantitatively accurate and experimentally verifiable predictions of alloys and alloy-substrate combinations, as well as the types, periodicities, and thermal stability of the resulting patterns.

B. Formalism

The general expression for the energetics of a pseudomorphic alloy film on an elastically stiff substrate can be written within the formalism of Ref. 28 as follows:

$$H = \frac{1}{2}\sum_i A_i^{\alpha\beta} u_i^\alpha u_i^\beta + \frac{1}{4}\sum_{i,j} k_{ij}[(u_i^\alpha - u_j^\alpha)e_{ij}^\alpha - \Delta_{ij}]^2 + \frac{1}{2}\sum_{i,j} J_{ij}^{\text{chem}} S_i S_j + H_{\text{sub}}, \tag{3}$$

where the indices i and j refer to binding sites on the substrate, while the Greek indices (α and β) denote Cartesian components (x and y) parallel to the substrate surface. Throughout the remainder of this section, summation over repeated Cartesian indices is implied. The physical interpretation of each of the terms in Eq. (3) is schematically illustrated in Fig. 2. The interaction of the film atoms with the substrate is described by the first term as a harmonic potential, where $A_i^{\alpha\beta}$ is the second derivative of the energy as a function of the *lateral* displacement (u_i) of a film atom at site i, which is away from the ideal binding site (it can be shown that the perpendicular component can be integrated out, see footnote 16 in Ref. 28). The second term in Eq. (3) represents the expression for the elastic energy of the atoms within the film, which is written in terms of a harmonic central-force potential, with k_{ij} denoting a force constant, e_{ij}^α representing the components of the unit vector connecting sites i and j, and Δ_{ij} parametrizing the strain in the i-j bond. The third term in Eq. (3) describes the "chemical" energy, which is given in the form of an Ising-model Hamiltonian, where S_i takes values of +1 or −1 for Ag or Fe atoms occupying site i, respectively, and J_{ij}^{chem} are effective-pair interactions [defined by Eq. (1)]. The final term represents the reduction in the energy of the combined (film+substrate) system associated with substrate deformations, which is in response to the distribution of surface forces ($\mathbf{F_i}$) arising from the lateral displacements of the film atoms. This term will be discussed in further detail below. In what follows, we refer to the sum of the first three terms of Eq. (3), representing the energy of the alloy film on a rigid, undeformed substrate as H_{film}.

In the application of Eq. (3) to Fe-Ag alloys on Ru(0001) and Mo(110) substrates, we introduce the following simplifying assumptions, which are justified below by the ability of the model to accurately describe first-principles calculated formation energies in these systems:

(i) The chemical interactions are assumed to take nonzero values, $J_{ij}^{\text{chem}} = J^{\text{chem}}$, for nearest-neighbor pairs only.

(ii) The substrate potential is assumed to be diagonal, $A_i^{xx} = A_i^{yy} = A$, with a magnitude (A) that is independent of the species occupying site i.

(iii) The force constants are assumed to couple only nearest-neighbor pairs and to have the same values, $k_{ij} = k$, independent of the bond type.

(iv) Based on the relative values of the atomic radii, it is expected that on both Mo(110) and Ru(0001) surfaces, Fe-Fe and Ag-Ag bonds should be under tensile and compressive strains, respectively, while Fe-Ag bonds are matched well to the substrate lattice spacing. We thus assume a simple parametrization for the bond strains: $\Delta_{ij} = \Delta(S_i + S_j)/2$. With this parametrization, the equilibrium bond lengths for Fe-Fe, Fe-Ag, and Ag-Ag bonds are $r_0 - \Delta$, r_0, and $r_0 + \Delta$, respectively, where r_0 denotes the nearest-neighbor distance on the substrate surface.

With these assumptions, the first three terms in Eq. (3) can be rearranged to take the following form:[28,46,47]

$$H_{\text{film}} = H_0 + \frac{1}{2}\sum_{i,j} J_{ij} S_i S_j + \frac{1}{2}\sum_{i,j} \Phi_{ij}^{\alpha\beta} u_i^\alpha u_j^\beta + \sum_{i,j} \Gamma_{ij}^\alpha u_i^\alpha S_j. \tag{4}$$

In Eq. (4), $H_0 = \frac{kZN\Delta^2}{8}$, where Z is the coordination number (number of nearest-neighbor sites within the alloy-film layer) and N is the total number of atoms in the alloy film. The second term contains contributions from both the chemical interactions and the elastic strain energy, i.e., $J_{ij} = J^{\text{chem}} + J^{\text{strain}}$, where $J^{\text{strain}} = \frac{k\Delta^2}{4}$. The combination of terms

$H_0+\frac{1}{2}\Sigma_{i,j}J^{\text{strain}}S_iS_j$ represents the configuration-dependent stored elastic strain energy in the *unrelaxed* monolayer film. The third and fourth terms in Eq. (4), which are associated with the film-atom displacements u_i, contribute to the elastic relaxation energy. The symbol $\Phi_{ij}^{\alpha\beta}$ denotes the force-constant tensor for the film atoms, and Γ_{ij}^{α} is the so-called Kanzaki-force term;[48] the product $-\Gamma_{ij}^{\alpha}S_j$ represents the force on atom i in the direction α due to the presence of atom type S_j at site j. In Sec. II C, explicit expressions for $\Phi_{ij}^{\alpha\beta}$ and Γ_{ij}^{α} are given for Fe-Ag/Ru(0001) and Fe-Ag/Mo(110) in terms of the parameters A, k, and Δ introduced above.

In applications of Eqs. (3) and (4), we eliminate the displacement variables (u_i) by invoking the condition of mechanical equilibrium. This task is simplified by making use of 2D lattice Fourier transforms defined as follows:[28]

$$S(\mathbf{q}) = \frac{1}{N}\sum_i S_i \exp(-i\mathbf{q}\cdot\mathbf{R_i}),$$

$$u_\alpha(\mathbf{q}) = \frac{1}{N}\sum_i u_i^\alpha \exp(-i\mathbf{q}\cdot\mathbf{R_i}),$$

$$J(\mathbf{q}) = \sum_j J_{ij} \exp(-i\mathbf{q}\cdot\mathbf{R_j}),$$

$$\Phi_{\alpha\beta}(\mathbf{q}) = \sum_j \Phi_{ij}^{\alpha\beta} \exp(-i\mathbf{q}\cdot\mathbf{R_j}),$$

$$\Gamma_\alpha(\mathbf{q}) = \sum_j \Gamma_{ij}^{\alpha} \exp(-i\mathbf{q}\cdot\mathbf{R_j}). \quad (5)$$

In Eq. (5), Fourier transforms of real-space quantities are denoted by their functional dependence on the wave vector $\mathbf{q}=(q_x,q_y)$. From the definitions in Eq. (5), the energy in Eq. (4) can be cast in the following form:

$$H_{\text{film}} = H_0 + \frac{N}{2}\sum_{\mathbf{q}} [u_\alpha^*(\mathbf{q})\Phi_{\alpha\beta}(\mathbf{q})u_\beta(\mathbf{q}) + 2S^*(\mathbf{q})\Gamma_\alpha(\mathbf{q})u_\alpha(\mathbf{q}) + J(\mathbf{q})|S(\mathbf{q})|^2], \quad (6)$$

where the sum is over all wave vectors within the (two-dimensional) Brillouin zone of the surface lattice, and the superscript $*$ denotes complex conjugates, with $S^*(\mathbf{q})=S(-\mathbf{q})$ and $u_\alpha^*(\mathbf{q})=u_\alpha(-\mathbf{q})$.

In the stiff-substrate limit,[28] the equilibrium values of the dísplacements of the film atoms are derived by the minimization of H_{film}. The equation of $\frac{\partial H_{\text{film}}}{\partial u_\alpha^*(\mathbf{q})}=0$ yields the following relation:

$$u_\alpha(\mathbf{q}) = -S(\mathbf{q})\Phi_{\alpha\beta}^{-1}(\mathbf{q})\Gamma_\beta(-\mathbf{q}), \quad (7)$$

where $\Phi_{\alpha\beta}^{-1}$, which is the inverse of the 2×2 force-constant matrix, represents a lattice Green's function. When the above expression for the displacements is inserted back into Eq. (6), the following expression is obtained for the total energy of the film:

$$H_{\text{film}} = H_0 + \frac{N}{2}\sum_{\mathbf{q}} J(\mathbf{q})|S(\mathbf{q})|^2 - \frac{N}{2}\sum_{\mathbf{q}} [\Gamma_\alpha(\mathbf{q})\Phi_{\alpha\beta}^{-1}(\mathbf{q})\Gamma_\beta^*(\mathbf{q})] \times |S(\mathbf{q})|^2. \quad (8)$$

In this equation, the sum of the first and second terms, which include both chemical and elastic contributions, represents the total energy of an epitaxially strained film that is completely coherent with the substrate, i.e., where all the atoms directly sit on the lattice sites of the underlying substrate and all displacements are zero ($\mathbf{u_i}=0$ for all i); the third term is negative and represents the elastic relaxation energy (i.e., reduction in elastic energy) arising when atoms are allowed to displace away from the ideal lattice sites to minimize the total energy. In the second term in Eq. (8), $J(\mathbf{q})$ gives rise to a short-ranged (nearest neighbor in this case) contribution to the effective-pair interactions in real space, while the bracketed expression in the third term yields a "medium-ranged" contribution to the interactions, originating from the exponentially decaying displacement fields in the Frenkel–Kontorova model.[28]

To summarize, the energy of the alloy film on a rigid substrate can be written in the form of a generalized Ising model Hamiltonian, which is expressed in reciprocal space, as follows:

$$H_{\text{film}} = H_0 + \frac{N}{2}\sum_{\mathbf{q}} J_{\text{film}}(\mathbf{q})|S(\mathbf{q})|^2, \quad (9)$$

where the ordering potential, $J_{\text{film}}(\mathbf{q})=J_{\text{chem}}(\mathbf{q})+J_{\text{elastic}}(\mathbf{q})$, contains contributions from both chemical [$J_{\text{chem}}(\mathbf{q})$, the Fourier transform of J^{chem}] and elastic [$J_{\text{elastic}}(\mathbf{q})$] interactions. The elastic interactions can be further divided into two contributions: $J_{\text{elastic}}(\mathbf{q})=J_{\text{strain}}(\mathbf{q})+J_{\text{relax}}(\mathbf{q})$, where $J_{\text{strain}}(\mathbf{q})$ is the Fourier transform of J^{strain}, and $J_{\text{relax}}(\mathbf{q})=-\Gamma_\alpha(\mathbf{q})\Phi_{\alpha\beta}^{-1}(\mathbf{q})\Gamma_\beta^*(\mathbf{q})$, which corresponds to the strain-induced interactions associated with the elastic relaxation energy.

We now consider the final term in Eq. (3) associated with elastic deformations of the substrate. To appreciate the significance of this term, it should be noted that in the derivation of the elastic energy contributions to Eq. (9), it was assumed that the substrate was rigid, i.e., displacements of the subsurface substrate atoms were neglected. In first-principles calculations of the energetics of periodic surface structures with modulation wavelengths on the order of a few nanometers (e.g., Refs. 28 and 44), this rigid-substrate assumption has been found to be highly accurate. At increasingly longer wavelengths, however, substrate displacements cannot be neglected. Consider as a specific example an Fe-Ag stripe superstructure with period Λ (cf. the right panel of Fig. 1). As Λ becomes very large on the scale of the interatomic spacing, the alternating patches of Fe and Ag can be viewed as representing stress domains, with the Fe/Ag interfaces giving rise to discontinuities in surface stress. At large composition-modulation wavelengths, the elastic relaxation energy arising from these surface forces should be described well by the continuum theory of elastically strained surfaces[30,41] described in Sec. II A. In this long-wavelength limit, elastic relaxations give rise to long-ranged subsurface

displacements within the substrate, which are neglected in the development of Eq. (9). Within the stiff-substrate limit defined in Ref. 28, the contribution of substrate deformations to the elastic relaxation energy can be incorporated through the substrate term H_{sub} in Eq. (3) defined as follows.

The contribution to the relaxation energy arising from substrate displacements can be regarded as a consequence of the response of the substrate to a surface force distribution resulting from displacements of the atoms within the film. Specifically, from Ref. 28, this force distribution is expressed as $F_\alpha = A u_\alpha$. The Fourier transform of this force distribution can thus be expressed using Eq. (7) as

$$F_\alpha(\mathbf{q}) = -A\Phi^{-1}_{\alpha\beta}(\mathbf{q})\Gamma_\beta(-\mathbf{q})S(\mathbf{q}). \tag{10}$$

According to the continuum theory of elastically strained surfaces,[30,41,49] the relaxation of such a surface force distribution leads to a net reduction in elastic energy:

$$H_{\mathrm{sub}} = -\frac{1}{2}\int\int p_\alpha(\mathbf{r})G_{\alpha\beta}(\mathbf{r}-\mathbf{r}')p_\beta(\mathbf{r}')d^2\mathbf{r}d^2\mathbf{r}', \tag{11}$$

where p is the force density (force per unit area), the two-dimensional integrals are over the surface, and $G_{\alpha\beta}(\mathbf{r}-\mathbf{r}')$ is the elastic Green's function for the semi-infinite substrate, which is evaluated on the surface. We assume that the continuous force distribution in Eq. (11) can be discretized in terms of the forces on each atom divided by the area per atom. With this assumption and making use of 2D Fourier transforms, Eq. (11) can be expressed as follows:

$$H_{\mathrm{sub}} = -\frac{N}{2S_0}\sum_{\mathbf{q}} F^*_\alpha(\mathbf{q})G_{\alpha\beta}(\mathbf{q})F_\beta(\mathbf{q}), \tag{12}$$

where S_0 is the surface area per atom. By making use of the expression for $F_\alpha(\mathbf{q})$ given in Eq. (10), we can rewrite Eq. (12) as follows:

$$H_{\mathrm{sub}} = \frac{N}{2}\sum_{\mathbf{q}} V_{\mathrm{sub}}(\mathbf{q})|S(\mathbf{q})|^2, \tag{13}$$

where

$$V_{\mathrm{sub}}(\mathbf{q}) = -\frac{A^2}{S_0}\{[\Phi^{-1}_{\alpha\gamma}(-\mathbf{q})\times\Gamma_\gamma(-\mathbf{q})]\times G_{\alpha\beta}(\mathbf{q}) \times[\Phi^{-1}_{\beta\delta}(\mathbf{q})\times\Gamma_\delta(\mathbf{q})]\}. \tag{14}$$

Thus, Eq. (14) shows that the substrate contribution to Eq. (3) leads to an additional contribution to the reciprocal-space interaction potential, which can be added to the terms $J_{\mathrm{chem}}(\mathbf{q})$ and $J_{\mathrm{elastic}}(\mathbf{q})$ given above. In the limit of long wavelengths ($\mathbf{q}\to 0$), it can be shown[28] that the magnitude of $V_{\mathrm{sub}}(\mathbf{q})$ vanishes, although the slope approaches the origin with a finite value that generally (for an elastically anisotropic substrate) depends on the direction of $\mathbf{q}$. This singular behavior gives rise to a long-ranged dipolar contribution to the interactions between film atoms, decaying with distance as r^{-3}.

To summarize the results of this section, we consider the formation energy of an alloy-film superstructure:

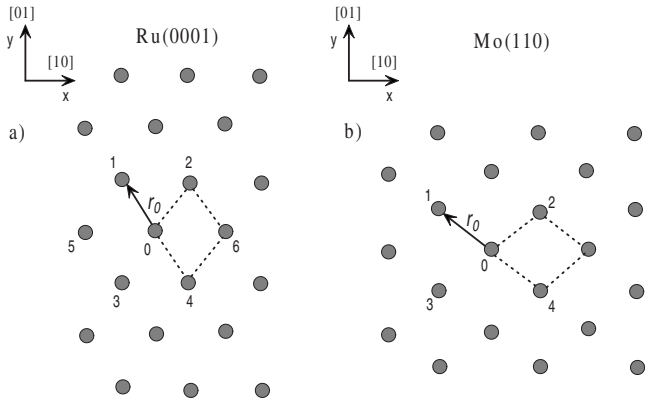

FIG. 3. Surface lattice structures for (a) Ru(0001) and (b) Mo(110) substrates. The six NNs for Ru and four for Mo are indicated. The coordinate systems used in this work for each substrate are described: for Ru(0001), x ([10]) and y ([01]) correspond to the $[01\bar{1}0]$ and $[\bar{2}\bar{1}30]$ directions in the crystal, respectively; for Mo(110), x ([10]) and y ([01]) correspond to the $[\bar{1}10]$ and [001] directions, respectively.

$$\Delta H = H - x_{\mathrm{Fe}}H(\mathrm{Fe}) - (1-x_{\mathrm{Fe}})H(\mathrm{Ag}), \tag{15}$$

where x_{Fe} is the mole fraction of Fe in the film, $H(\mathrm{Fe})$ is the energy of a pure-Fe film and, $H(\mathrm{Ag})$ corresponds to a pure-Ag film. From the results given above, this formation energy can be cast in the form of an Ising model Hamiltonian,

$$\Delta H = \frac{N}{2}\sum_{\mathbf{q}} V(\mathbf{q})|S(\mathbf{q})|^2, \tag{16}$$

where the interaction potential is given in terms of film and substrate contributions as

$$V(\mathbf{q}) = V_{\mathrm{film}}(\mathbf{q}) + V_{\mathrm{sub}}(\mathbf{q}), \tag{17}$$

with $V_{\mathrm{film}}(\mathbf{q}) = J_{\mathrm{film}}(\mathbf{q}) - J_{\mathrm{film}}(\mathbf{q}=0)$. In Sec. IV, the nature of the competing interactions underlying the stability of nanometer-scale modulated alloy superstructures will be discussed in terms of the elastic and chemical contributions to the interaction potential, i.e.,

$$V_{\mathrm{film}}(\mathbf{q}) = V_{\mathrm{chem}}(\mathbf{q}) + V_{\mathrm{elastic}}(\mathbf{q}), \tag{18}$$

where

$$V_{\mathrm{chem}}(\mathbf{q}) = J_{\mathrm{chem}}(\mathbf{q}) - J_{\mathrm{chem}}(\mathbf{q}=0) \tag{19}$$

and

$$V_{\mathrm{elastic}}(\mathbf{q}) = J_{\mathrm{elastic}}(\mathbf{q}) - J_{\mathrm{elastic}}(\mathbf{q}=0) \tag{20}$$

in terms of the elastic and chemical interactions defined above.

C. Parametrization for Fe-Ag on Ru(0001) and Mo(110)

In this section, we consider the geometry of Ru(0001) and Mo(110) surfaces and provide detailed expressions for $\Phi_{\alpha\beta}(\mathbf{q})$, $\Gamma_\alpha(\mathbf{q})$, $J(\mathbf{q})$, and $G_{\alpha\beta}(\mathbf{q})$ in terms of the four model parameters: A, k, J^{chem}, and Δ, which were defined above.

1. Hamiltonian for Fe-Ag/Ru(0001)

The adsorption sites on the Ru(0001) surface form a hexagonal lattice with six nearest neighbors, as illustrated in Fig. 3(a). The unit cell vectors are chosen as $(\frac{1}{2}r_0, -\frac{\sqrt{3}}{2}r_0)$ and $(\frac{1}{2}r_0, \frac{\sqrt{3}}{2}r_0)$, where r_0 is the nearest-neighbor distance. By considering the geometry of the lattice, H_{film} in Eq. (3) can be written as follows:

$$H_{\text{film}} = H_0 + \frac{1}{2}\sum_{i,j}\left(\frac{k\Delta^2}{4} + J^{\text{chem}}\right)S_iS_j + \frac{1}{2}\sum_{i,j}\{[A+3k]\delta_{ij}[u_i^\alpha]^2 - ku_i^\alpha E_{ij}^{\alpha\beta}u_j^\beta\} + \frac{1}{2}\sum_{i,j}k\Delta S_i(e_{ij}^\alpha u_j^\alpha), \tag{21}$$

where δ_{ij} is 1 if $i=j$ and 0 if $i\neq j$, and

$$E_{ij} = \begin{bmatrix} (e_{ij}^x)^2 & e_{ij}^x e_{ij}^y \\ e_{ij}^x e_{ij}^y & (e_{ij}^y)^2 \end{bmatrix}.$$

From Eq. (21), the following expressions can be derived for the terms making up the interaction potential $V_{\text{film}}(\mathbf{q})$:

$$\Phi_{xx}(\mathbf{q}) = (A+3k) - k\left[2\cos(q_x r_0) + \cos\left(\frac{q_x r_0}{2}\right)\cos\left(\frac{\sqrt{3}}{2}q_y r_0\right)\right],$$

$$\Phi_{yy}(\mathbf{q}) = (A+3k) - 3k\cos\left(\frac{q_x r_0}{2}\right)\cos\left(\frac{\sqrt{3}}{2}q_y r_0\right),$$

$$\Phi_{xy}(\mathbf{q}) = \Phi_{yx}(\mathbf{q}) = \sqrt{3}k\sin\left(\frac{q_x r_0}{2}\right)\sin\left(\frac{\sqrt{3}}{2}q_y r_0\right),$$

$$\Gamma_x(\mathbf{q}) = -ik\Delta\left[\sin(q_x r_0) + \sin\left(\frac{q_x r_0}{2}\right)\cos\left(\frac{\sqrt{3}}{2}q_y r_0\right)\right],$$

$$\Gamma_y(\mathbf{q}) = -i\sqrt{3}k\Delta\cos\left(\frac{q_x r_0}{2}\right)\sin\left(\frac{\sqrt{3}}{2}q_y r_0\right),$$

$$J(\mathbf{q}) = (k\Delta^2 + 4J^{\text{chem}})\cos\left(\frac{q_x r_0}{2}\right)\left[\cos\left(\frac{q_x r_0}{2}\right) + \cos\left(\frac{\sqrt{3}}{2}q_y r_0\right)\right]. \tag{22}$$

As in Ref. 28, we calculate $V_{\text{sub}}(\mathbf{q})$ by using isotropic elasticity theory.[49] The Green's function in Eq. (14) thus takes the following form in reciprocal space:

$$G_{xx}(\mathbf{q}) = \frac{2(1-\nu^2)}{E}\frac{1}{|\mathbf{q}|} + \frac{2\nu(1+\nu)}{E}\frac{q_y^2}{|\mathbf{q}|^3},$$

$$G_{yy}(\mathbf{q}) = \frac{2(1-\nu^2)}{E}\frac{1}{|\mathbf{q}|} + \frac{2\nu(1+\nu)}{E}\frac{q_x^2}{|\mathbf{q}|^3},$$

$$G_{xy}(\mathbf{q}) = G_{yx}(\mathbf{q}) = -\frac{2\nu(1+\nu)}{E}\frac{q_x q_y}{|\mathbf{q}|^3}, \tag{23}$$

where $|\mathbf{q}| = \sqrt{q_x^2+q_y^2}$, ν is Poisson's ratio, and E is Young's modulus of bulk Ru.

2. Hamiltonian for Fe-Ag/Mo(110)

Elemental Mo has a body-centered cubic (bcc) structure and the Mo(110) surface is illustrated in Fig. 3(b). In the surface plane, a primitive unit cell is defined with unit cell vectors $(\frac{\sqrt{6}}{3}r_0, \frac{\sqrt{3}}{3}r_0)$ and $(\frac{\sqrt{6}}{3}r_0, -\frac{\sqrt{3}}{3}r_0)$, where r_0 is the nearest-neighbor distance. By considering the geometry of the surface, H_{film} in Eq. (3) can be written as follows:

$$H_{\text{film}} = H_0 + \frac{1}{2}\sum_{i,j}\left(\frac{k\Delta^2}{4} + J^{\text{chem}}\right)S_iS_j + \frac{1}{2}\sum_{i,j}\left\{\left[A+\frac{8}{3}k\right]\delta_{ij}(u_i^x)^2 + \left[A+\frac{4}{3}k\right]\delta_{ij}(u_i^y)^2 - ku_i^\alpha E_{ij}^{\alpha\beta}u_j^\beta\right\} + \frac{1}{2}\sum_{i,j}k\Delta S_i(e_{ij}^\alpha u_j^\alpha). \tag{24}$$

Accordingly, the following expressions can be derived for the terms composing the interaction potential $V_{\text{film}}(\mathbf{q})$:

$$\Phi_{xx}(\mathbf{q}) = \left(A+\frac{8}{3}k\right) - \frac{8}{3}k\cos\left(\sqrt{\frac{2}{3}}q_x r_0\right)\cos\left(\sqrt{\frac{1}{3}}q_y r_0\right),$$

$$\Phi_{yy}(\mathbf{q}) = \left(A+\frac{4}{3}k\right) - \frac{4}{3}k\cos\left(\sqrt{\frac{2}{3}}q_x r_0\right)\cos\left(\sqrt{\frac{1}{3}}q_y r_0\right),$$

$$\Phi_{xy}(\mathbf{q}) = \Phi_{yx}(\mathbf{q}) = 4\sqrt{\frac{2}{9}}k\sin\left(\sqrt{\frac{2}{3}}q_x r_0\right)\sin\left(\sqrt{\frac{1}{3}}q_y r_0\right),$$

$$\Gamma_x(\mathbf{q}) = -i2\sqrt{\frac{2}{3}}k\Delta\sin\left(\sqrt{\frac{2}{3}}q_x r_0\right)\cos\left(\sqrt{\frac{1}{3}}q_y r_0\right),$$

$$\Gamma_y(\mathbf{q}) = -i2\sqrt{\frac{1}{3}}k\Delta\cos\left(\sqrt{\frac{2}{3}}q_x r_0\right)\sin\left(\sqrt{\frac{1}{3}}q_y r_0\right),$$

$$J(\mathbf{q}) = (k\Delta^2 + 4J^{\text{chem}})\cos\left(\sqrt{\frac{2}{3}}q_x r_0\right)\cos\left(\sqrt{\frac{1}{3}}q_y r_0\right). \tag{25}$$

For $V_{\text{sub}}(\mathbf{q})$, we require an expression for the elastic Green's function. Unlike the case for Ru(0001), where isotropic elasticity is assumed, for the twofold symmetrical Mo(110) surface, we explicitly account for elastic anisotropy within the Stroh formalism[50] developed by Ting.[51] In the application of this formalism, we note that composition modulation along a particular direction $(\mathbf{q})$ gives rise to a one-dimensional force distribution on the substrate surface. Hence, the elastic field within the surface and substrate is two dimensional. Let y' denote the direction normal to the surface and pointing into

the substrate, while x' is the direction along the composition modulation ($\mathbf{q}$). The expression for $G_{x'x'}(\mathbf{q})$, required to calculate $V_{\mathrm{sub}}(\mathbf{q})$ in Eq. (14), is given as follows:

$$G_{x'x'}(\mathbf{q}) = \frac{1}{|\mathbf{q}|} \cdot (L^{-1}_{x'x'}), \tag{26}$$

where L^{-1} is the inverse of the L matrix defined in Ref. 52 in terms of the substrate single-crystal elastic constants in the $x'y'z'$ coordinate system, where z' is the direction parallel to the surface and perpendicular to $\mathbf{q}$.

III. COMPUTATIONAL DETAILS

In this section, we describe the details surrounding our calculation of the model parameters describing the interaction potential for equiatomic monolayer Fe-Ag alloys on Ru(0001) and Mo(110) substrates. Specifically, we provide details related to the first-principles calculations of substrate single-crystal elastic constants (for the elastic Green's functions), short-period formation energies for Fe_nAg_n stripe structures, and differences in surface stress between systems with pure-Fe or -Ag films on each substrate. Results for each of these quantities are presented, and we describe how the values of the model parameters A, J^{chem}, k, and Δ are derived by fitting to the calculated formation energies and surface stresses. This section ends with a brief discussion on how the resulting model interaction potentials are used in Monte Carlo (MC) simulations as a framework for investigating stripe-ordering tendencies at finite temperatures.

A. First-principles calculations

All of the first-principles calculations reported in this work were performed within the framework of DFT by employing ultrasoft pseudopotentials (USPPs),[53] as implemented in the Vienna *ab initio* simulation package (VASP).[54,55] Calculations were performed by employing the 1991 generalized gradient approximation of Perdew and Wang[56] and the pseudopotentials labeled "Mo," "Ru," "Fe," and "Ag" in the VASP library. All calculations involving Fe were performed spin polarized. Calculations for Mo and Ru elastic constants followed standard procedures,[57] employing plane-wave cutoffs of 297 eV for Mo and 237.5 eV for Ru, and k-point meshes of $20\times20\times20$ for Mo and $12\times12\times12$ for Ru. The calculations yield the following results for the lattice constants (a and c/a) and single-crystal elastic moduli (C_{ij}). For Mo: $a=3.15$ Å, $r_0=\frac{\sqrt{3}}{2}a=2.728$ Å, $C_{11}=2.86$ eV/Å^3, $C_{12}=0.95$ eV/Å^3, and $C_{44}=0.58$ eV/Å^3; for Ru: $a=2.728$ Å, $r_0=a=2.728$ Å, $c/a=1.583$, $C_{11}=5.54$ eV/Å^3, $C_{12}=1.74$ eV/Å^3, $C_{13}=1.64$ eV/Å^3, $C_{33}=6.16$ eV/Å^3, and $C_{44}=1.79$ eV/Å^3. For Mo, the results agree to within 5% of experimental measurements for C_{11} and C_{12}, and within 17% for C_{44},[58] while for Ru, all elastic constants are within 7% of the experimentally determined values.[59]

First-principles calculations for short-period Fe_nAg_n stripe superstructures, which are modulated along the [10] and [01] directions on Ru(0001) and Mo(110) substrates, were computed by employing slab supercell geometries. The slabs were composed of six substrate layers wherein the positions of the atoms on the bottom two layers were held fixed at their ideal crystal sites (all other atoms were allowed to relax). The top substrate layer was covered either by pure-Fe or -Ag films, or by pseudomorphic Fe_nAg_n superstructures. The two surfaces (top and bottom) were separated by vacuum that is three layers thick (~6.7 Å). In these calculations, a plane-wave cutoff of 236.5 eV was used for systems on Mo(110) and 237.5 eV for Ru(0001). The k-point sampling was performed by using a single point in the direction normal to the surface, and meshes equivalent to 6×8 for the rectangular (two-atom) unit cell on Mo(110) and 12×12 for the rectangular (two-atom) unit cell on Ru(0001). Convergence tests with respect to plane-wave cutoff, k-point density, and slab and vacuum thicknesses were performed, indicating that the formation energies for the Fe_nAg_n stripes with periodicities up to $n=8$ are converged to within a few meV/atom. Some additional calculations were also undertaken to test the accuracy of the US pseudopotentials used in this work. For FeAg on Mo(110), independent calculations were performed with VASP using the projector-augmented wave method[60,61] with the Fe, Ag, and Mo PW91 potentials; the converged formation energy for this structure was found to agree to within 2 meV/atom of the results obtained with USPPs. The results for the calculated formation energy of Fe_nAg_n stripes on Ru(0001) and Mo(110) are given in Table I and are discussed further below.

TABLE I. Calculated stripe formation energies ΔH (in units of eV/atom) in two principal modulation directions.

	Fe-Ag/Ru(0001)		Fe-Ag/Mo(110)	
Stripe period	[10]	[01]	[10]	[01]
Fe_1Ag_1	−0.0148	−0.0148	0.101	0.101
Fe_2Ag_2	−0.039	−0.0954	0.002	0.0017
Fe_3Ag_3	−0.0762	−0.1114	−0.024	−0.0225
Fe_4Ag_4	−0.0973	−0.1127	−0.03	−0.0203
Fe_5Ag_5			−0.0354	−0.0219
Fe_6Ag_6	−0.1094	−0.0958	−0.034	−0.0212
Fe_8Ag_8			−0.032	

As discussed in Ref. 28, the long-wavelength (small-$\mathbf{q}$) behavior of $V(\mathbf{q})$ is determined by the difference ($\delta\sigma$) between the intrinsic surface stress for a substrate covered by a pure-Fe pseudomorphic film (σ_{Fe}) versus a pure-Ag film (σ_{Ag}). To accurately parametrize the small-$\mathbf{q}$ behavior of $V(\mathbf{q})$, first-principles calculations of $\delta\sigma$ have been undertaken as follows. For the Mo(110) system, we employed a symmetric slab geometry containing 11 layers of Mo, with pure-Fe or pure-Ag films on both the top and bottom; the two films were separated by eight vacuum layers. Calculations of the stress tensor were undertaken by employing a plane-wave cutoff of 400 eV and a k-point density of $17\times17\times1$, corresponding to the primitive unit cell illustrated in Fig. 3(b). The structure was relaxed, fixing the in-plane lattice constant to the value corresponding to unstrained bulk Mo. From the resulting components of the calculated stress tensor (multiplied by the periodic length of the slab supercell normal to

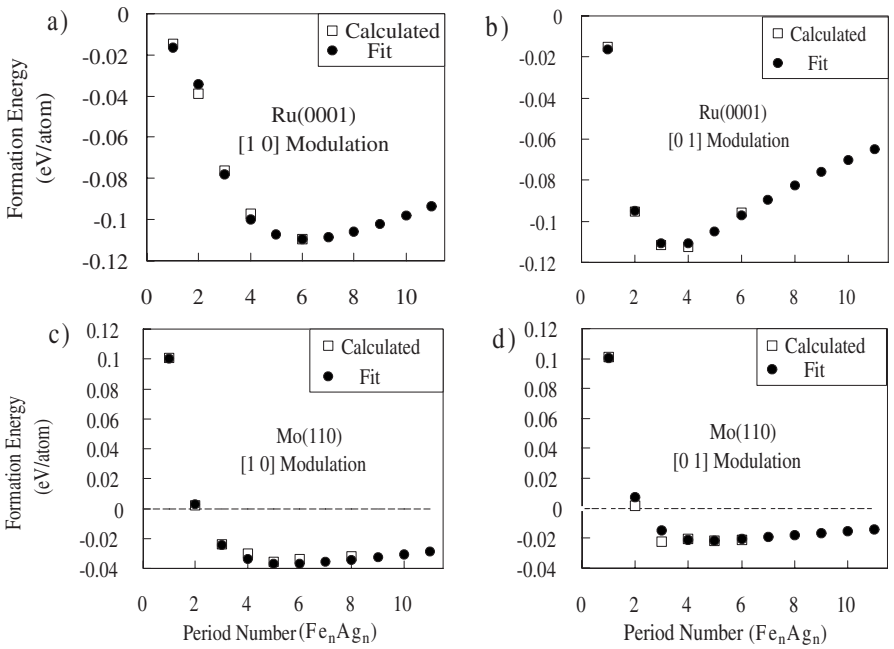

FIG. 4. Comparison between first-principles calculations and model predictions for the formation energies of Fe_nAg_n stripe structures on [(a) and (b)] Ru(0001) and [(c) and (d)] Mo(110). The modulation directions in (a) and (c) are along the [10] directions defined in Fig. 3, while (b) and (d) are for [01] modulation directions.

the surface and divided by 2 to account for the two surfaces), we computed the *xx* and *yy* components of the surface stress tensor, yielding $\delta\sigma_{xx}=0.38$ eV/Å^2 and $\delta\sigma_{yy}=0.24$ eV/Å^2. For the Ru(0001) system, where the surface stress tensor is isotropic, a similar procedure was followed. By using a plane-wave cutoff of 400 eV and a *k*-point density of 12×12, we computed $\delta\sigma=0.52$ eV/Å^2 for the difference between the trace of surface stress for Fe and Ag films. From tests involving the use of higher *k*-point densities, different slab thicknesses, and direct calculations of the surface stresses from the variations in energy as a function of applied strain, these numbers are estimated to be converged to a precision within 10%.

B. Fitting of model parameters

The values of the interaction-potential parameters, namely, A, k, J^{chem}, and Δ, are derived by fitting to the first-principles results described above, as follows. The difference in surface stress for substrates covered by Fe versus Ag thin films can be related to the model parameters by using Eq. (3). Considering first the Ru(0001) substrate, we note that the surface stress tensor for this system is isotropic; let σ_{Fe} and σ_{Ag} denote the trace of the surface stress ($S_0\frac{\partial\gamma}{\partial S}$, where γ is the surface energy and S_0 denotes the surface area per atom) for a Ru(0001) substrate with a pseudomorphic film of Fe or Ag, respectively. From Eq. (3), the difference of $\delta\sigma=\sigma_{\text{Fe}}-\sigma_{\text{Ag}}$ can be related to the model parameters as $\delta\sigma=\frac{2\sqrt{3}k\Delta}{r_0}$. Similarly, for Mo(110), where the surface stress is anisotropic, let $\delta\sigma_{[10]}$ and $\delta\sigma_{[01]}$ denote the difference in the *xx* and *yy* components of the surface stress, respectively, between systems with pure-Fe and -Ag films. From Eq. (3), the following relations can be derived: $\delta\sigma_{[10]}=\frac{2\sqrt{2}k\Delta}{r_0}$, $\delta\sigma_{[01]}=\frac{\sqrt{2}k\Delta}{r_0}$.

To fit the four parameters A, k, J^{chem}, and Δ, we perform a least-squares fit of (i) the model Hamiltonian to the relaxed stripe-structure formation energies given in Table I and (ii) the relationships involving surface stress described above, leading to the additional relation of $k\Delta=0.41$ eV/Å for Ru(0001) and $k\Delta=0.42$ eV/Å for Mo(110). The fits are nonlinear and are performed by using a downhill simplex method.[62] The quality of the fits is indicated in Fig. 4, which compares the calculated and model predictions for short-period Fe_nAg_n stripe formation energies. It is seen that the four-parameter model is able to reproduce the first-principles calculated formation energies to within a few meV/atom. Additionally, for Fe_nAg_n stripe structures on Mo(110), the model accurately reproduces the feature that the lowest formation energy corresponds to stripes modulated along the [10] direction, and the minimum in ΔH for values of n around 5 is also reproduced. For Ru(0001), the model reproduces the nearly degenerate values of the minimum formation energies for $n\approx6$ and $n\approx4$ along the [10] and [01] directions, respectively.

The values of the model parameters resulting from the fitting procedure described above are listed in Table II. For

TABLE II. Least-squares fitted model parameters for the FeAg/Ru(0001) and FeAg/Mo(110) systems.

	A (eV/Å^2)	J^{chem} (eV)	k (eV/Å^2)	Δ (Å)	$\frac{k\Delta^2}{4}$ (eV)
Ru(0001)	0.319	−0.177	0.879	0.469	0.048
Mo(110)	0.561	−0.206	1.640	0.254	0.026

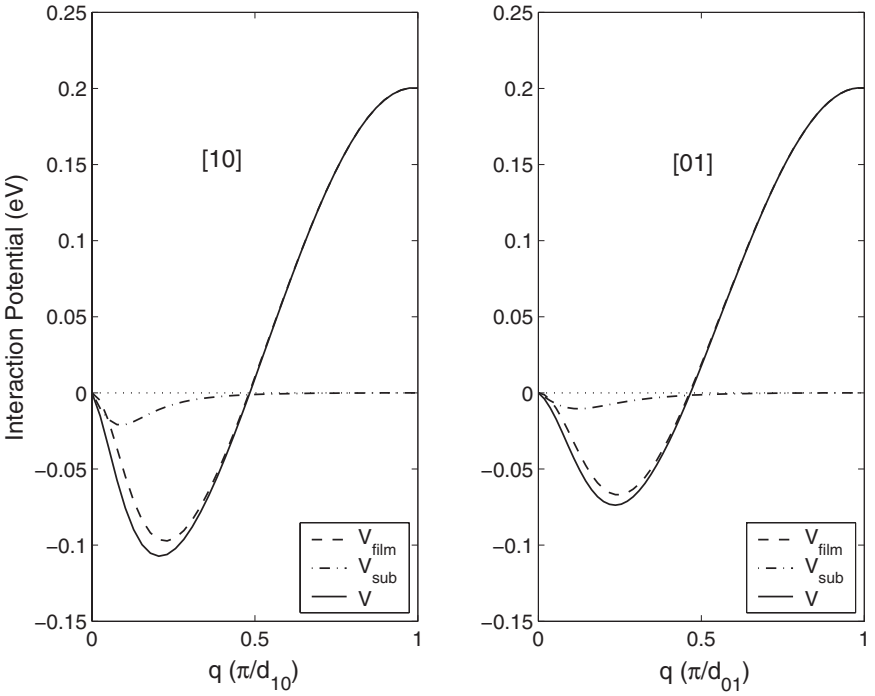

FIG. 5. V_{film}, V_{sub}, and V along the [10] and [01] directions. $d_{[10]}$ is the distance between adjacent Mo($\bar{1}$10) planes and $d_{[01]}$ is for Mo(001) planes.

both Ru(0001) and Mo(110), we obtain a value of J^{chem} that is negative and of the order of 0.2 eV; the large negative value is indicative of a strong chemically driven tendency to phase separate, which is consistent with the immiscibility observed in both the solid and liquid phases for bulk Fe-Ag alloys. The parameter A is found to be slightly larger for Mo than that for Ru, suggesting a slightly stronger binding between the film and the substrate in the former system. Also, the effective size mismatch, as reflected in the parameter Δ, is slightly lower for Mo relative to Ru, while the bond stiffness (k) shows the reverse trend. The stored elastic energy ($\frac{k\Delta^2}{4}$) is predicted to be roughly a factor of 2 larger on the Ru substrate, and for both systems, this energy is smaller in magnitude than the chemical interaction (J^{chem}).

C. Monte Carlo simulations

Finite-temperature structures and phase equilibria for FeAg films on Mo(110) and Ru(0001) substrates were investigated by employing Monte Carlo simulations in the semi-grand-canonical ensemble (i.e., an ensemble corresponding to a fixed number of surface atoms but with an overall composition that fluctuates consistent with a fixed value of the chemical potential difference between Fe and Ag). These simulations were based on the interaction potential $V(\mathbf{q})$ defined above, and each simulation began by tabulating the potential at each of the independent $\mathbf{q}$ vectors for the periodic simulation supercell by using the formulas and parameters given in Sec. II. The configurational degrees of freedom were sampled through single spin-flip "moves," which were accepted or rejected based on the Metropolis algorithm for a semi-grand-canonical ensemble with zero external field (i.e., zero chemical potential difference between Fe and Ag atoms, giving an average composition of $x_{\mathrm{Fe}}=1/2$ for the pairwise Hamiltonian). To speed up the calculations, when evaluating changes in energy associated with each Monte Carlo move, we employed a novel algorithm proposed by Lu *et al.*,[63] exploiting the use of fast-Fourier transforms. The system sizes employed for all the simulation results presented below were 128×128 primitive unit cells. Calculations were performed over a range of temperatures following a "simulated annealing" procedure whereby the temperature was sequentially decreased from a high temperature of 1700 to 10 K in steps of 10 K. At the highest temperature, the simulation was initiated from a random distribution of Fe and Ag atoms, while for all the other temperatures, the input structure was the final configuration from the previous temperature. For each temperature, Monte Carlo simulations ran for 10^5 steps per atom. A number of tests were conducted to examine the effects of system size, simulation time, and hysteresis. These tests involved running simulations with system sizes up to 256×256 and time scales up to 10^7 steps per atom. Over the range of temperatures for which results are presented below (1300–300 K), the system size and simulation times were found to be sufficiently large to give well-equilibrated results for equilibrium structures and heat capacities. At lower temperatures, however, long equilibration times and finite-size effects, which are exacerbated in some cases by the formation of stripe periodicities incommensurate with the periodic lengths of the simulation cell, complicated the investigation of thermodynamic properties and phase equilibria; further work is thus needed to characterize low-temperature phase equilibria and phase transitions for the Hamiltonians investigated here.

IV. RESULTS

In this section, we compare results for the energetics and finite-temperature equilibrium structures of Fe-Ag pseudomorphic monolayer films on Mo(110) and Ru(0001) sub-

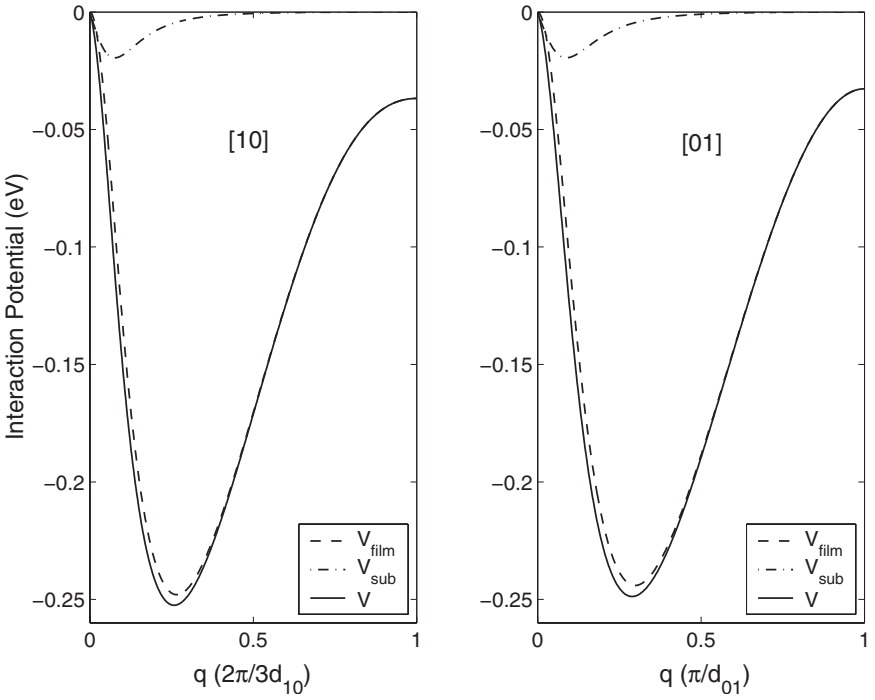

FIG. 6. V_{film}, V_{sub}, and V along the [10] and [01] directions. $d_{[10]}$ is the distance between adjacent Ru([01$\bar{1}$0]) planes and $d_{[01]}$ is for Ru ([$\bar{2}\bar{1}$30]) planes.

strates. We begin by considering the interaction potential $V(\mathbf{q})$ defined in Sec. III. In Figs. 5 and 6, $V(\mathbf{q})$ is plotted along the high-symmetry [10] and [01] directions for Mo and Ru, respectively. Also plotted are the individual contributions $V_{\text{film}}(\mathbf{q})$ and $V_{\text{sub}}(\mathbf{q})$ defined in Eq. (17). For both substrates, along each direction, minima in $V(\mathbf{q})$ are observed at wave vectors $\mathbf{q}$ corresponding to nanometer-scale composition modulations. Specifically, for Mo(110), the global minimum value of $V(\mathbf{q}_{\text{min}})=-0.107$ eV is obtained at $\mathbf{q}_{\text{min}}=[0.208\pi/d_{10},0]$, where d_{10} is the distance between atom rows along the [10] direction, corresponding to an optimal composition-modulation wavelength of $\Lambda_{\text{min}}=2.14$ nm; as described further below, this result is in good agreement with experimental observations[24] for this system. A comparison of the results for Mo(110) along the [10] versus the [01] directions shows a clear anisotropy in the ordering potential, with the [10] composition modulations favored at all finite wavelengths. For Ru(0001), the interaction potential is much more isotropic; a global minimum value of $V(\mathbf{q}_{\text{min}})=-0.253$ eV is obtained at a wave vector of $\mathbf{q}_{\text{min}}=[0.172\pi/d_{10},0]$ (and the five other wave vectors related by the symmetry of the surface), corresponding to a composition modulation along the [10] directions with a wavelength of $\Lambda_{\text{min}}=1.59$ nm, which is similar in magnitude but slightly smaller than that for the Mo(110) substrate.

For both Mo(110) and Ru(0001) substrates, the interaction potential $V(\mathbf{q})$ contains a dominant contribution from $V_{\text{film}}(\mathbf{q})$ for values of $\mathbf{q}$ with magnitudes comparable to and larger than $\mathbf{q}_{\text{min}}$. The substrate contribution $V_{\text{sub}}(\mathbf{q})$ is seen to significantly contribute to the potential only at relatively small values of $\mathbf{q}$, corresponding to modulation wavelengths several times larger than Λ_{min}. Since the ground-state structures are primarily determined by the magnitude of $V(\mathbf{q})$ near $\mathbf{q}=\mathbf{q}_{\text{min}}$, where it is dominated by $V_{\text{film}}(\mathbf{q})$, it is interesting to examine this contribution in further detail. In Figs. 7 and 8, we plot the chemical and elastic contributions to $V_{\text{film}}(\mathbf{q})$ for Mo and Ru, respectively, along one of the two high-symmetry modulation directions. As expected from the bulk phase diagram for Fe-Ag (which features pronounced immiscibility even in the liquid phase),[64] the chemical contribution $V_{\text{chem}}(\mathbf{q})$ is seen to have a minimum at $\mathbf{q}=0$, corresponding to macroscopic phase separation. By contrast, $V_{\text{elastic}}(\mathbf{q})$ has a minimum at $\pi/d=1$ in Figs. 7 and 8. Consequently, the elastic energy favors the formation of Fe-Ag bonds and is minimized for composition modulations corresponding to alternating atomic rows of Fe and Ag. Figures 7 and 8 serve to illustrate the competition between chemical and elastic interactions underlying the ordering energetics of Fe-Ag films on Mo and Ru substrates. In both cases, these contributions are found to be of comparable magnitudes, and their competing contributions lead to a minimum in $V_{\text{film}}(\mathbf{q})$, representing a compromise between chemistry (favoring macroscopic phase separation) and elasticity (favoring ordering); the result is a thermodynamically stable wavelength representing stable "phase separation" on the nanometer scale.

The nature of the effective-pair interactions in real space $[V(r)]$ is illustrated in Fig. 9, which plots chemical (J_{chem}) and elastically mediated contributions to $V(r)$ for the FeAg/Ru(0001) system. The elastically mediated interactions are further divided into the medium-ranged contributions associated with elastic displacements within the film layer ($V_{\text{film}}^{\text{elastic}}$) and the long-ranged substrate-mediated contributions ($V_{\text{sub}}^{\text{elastic}}$), derived, respectively, from inverse Fourier transforms of $V_{\text{elastic}}(\mathbf{q})$ and $V_{\text{sub}}(\mathbf{q})$ defined in Sec. II B. The dominant magnitudes of the nearest-neighbor chemical and medium-ranged elastic interactions are clearly apparent for r up to several nanometers. The inset in Fig. 9 plots the long-ranged tail of the effective-pair interactions on a semilogarithmic scale, showing that the substrate-mediated contributions $[V_{\text{sub}}]$ make a dominant contribution only at distances larger than about 4 nm, or approximately 15 times the nearest-neighbor spacing ($a=2.728$ Å). Beyond a distance

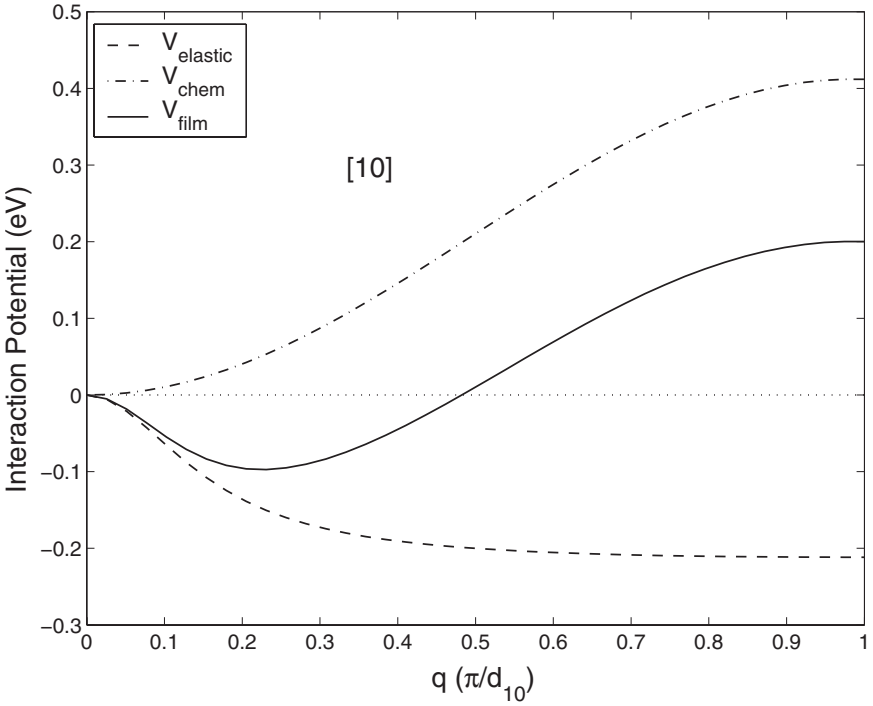

FIG. 7. V_{elastic}, V_{chem}, and V_{film} along the [10] direction. $d_{[10]}$ is the distance between adjacent Mo($\bar{1}$10) planes.

of $r \sim 15-20a$, the substrate-mediated contributions to the interactions are observed to give rise to the expected asymptotic dipolar scaling, $V(r) \sim 1/r^3$.

Next, we consider the finite-temperature stability of compositionally patterned phases for FeAg on Mo(110) and Ru(0001), which were investigated by MC simulations based on the interaction potentials given above. As described in Sec. III C, the MC simulations were performed by employing a simulated annealing procedure starting from a high temperature of 1300 K. The heat capacities (C_V) and snapshots obtained from these simulations are shown in Figs. 10–12. For both Mo and Ru substrates, the C_V results display clear signatures indicating the presence of phase transitions upon cooling.

For Mo(110), the broad character of the peak in the C_V plot is qualitatively consistent with a second-order transition. At high temperatures, the snapshots in Fig. 11 display a short-range ordered phase, which transforms to a lower-temperature ordered stripe phase at approximately 970 K. From examinations of the calculated structure factors for this phase, the dominant modulation wavelength for the low-temperature stripe structures is about 2.2 nm, corresponding

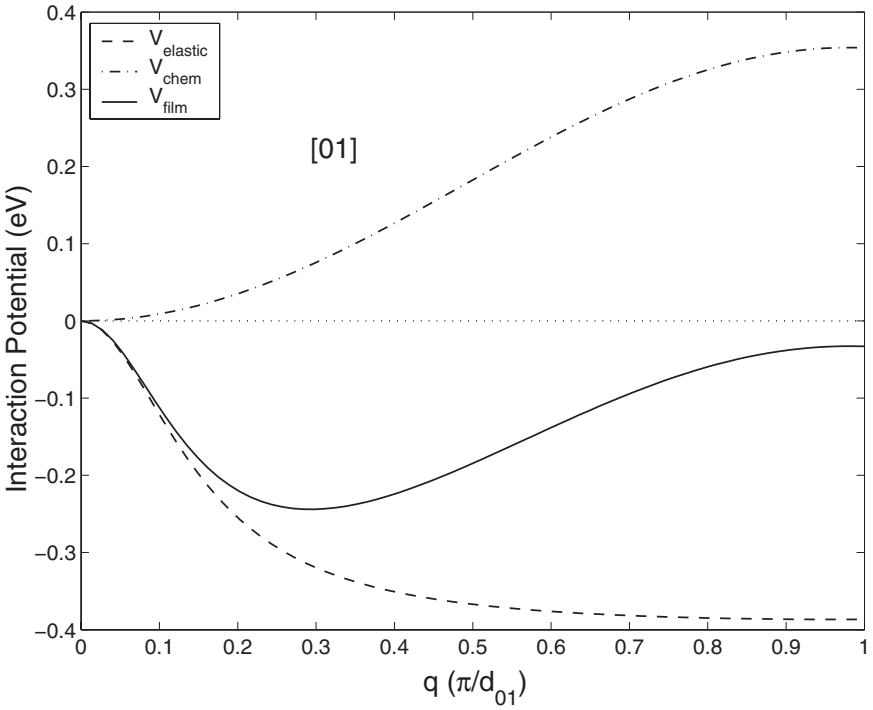

FIG. 8. V_{elastic}, V_{chem}, and V_{film} along the Ru[01] direction. $d_{[01]}$ is the distance between adjacent Ru([$\bar{2}\bar{1}$30]) planes.

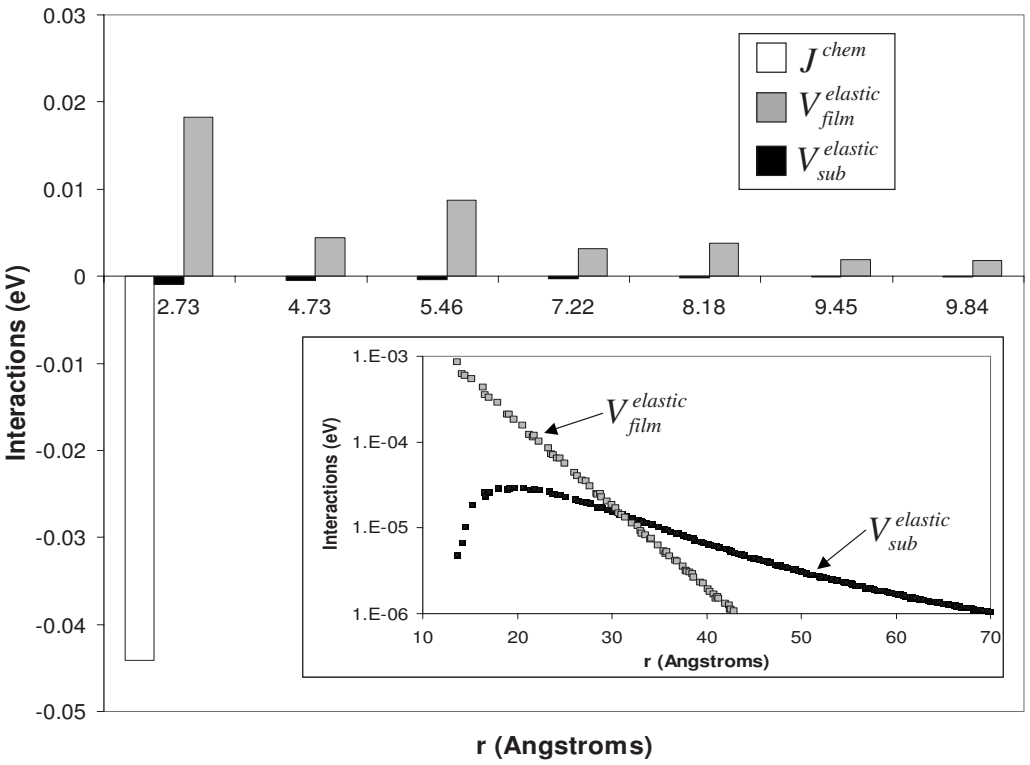

FIG. 9. Chemical (J^{chem}) and elastically mediated contributions to the real-space effective-pair interactions for FeAg/Ru(0001). The elastically mediated interactions are divided into the medium-ranged contributions arising from displacements within the alloy film ($V_{\text{film}}^{\text{elastic}}$) and the long-ranged contributions ($V_{\text{sub}}^{\text{elastic}}$) associated with substrate-mediated displacements. The inset plots the long-ranged tail of the elastically mediated interactions on a semilogarithmic scale.

most closely to a stripe phase with an Fe_5Ag_5 periodicity.

For the Ru substrate, the results in Figs. 10 and 12 display significant differences from those derived on Mo(110). Specifically, for Ru(0001), the C_V results show a relatively featureless behavior over the range of temperatures wherein the same alloy films on Mo(110) display a clear transition to a long-range-ordered stripe phase. In the temperature range between roughly 460 and 1300 K, interconnected, topologically disordered stripe structures are observed for the Fe-Ag/Ru(0001) films, as exemplified by the snapshot at 600 K in Fig. 12. At approximately 460 K, a relatively sharp ordering transition is obtained from the topogically disordered phase to a long-range-ordered stripe phase oriented along one of the symmetry-equivalent [10] directions. At much lower temperatures, it was observed that the [10] stripe phase undergoes a second transition in which the stripes change their direction to [01] orientations; results for this low-temperature transition are not presented here since we were unable to achieve fully equilibrated simulation data, which are free of hysteresis, in this temperature range.

V. DISCUSSION

For the FeAg/Mo(110) system, the predictions of the present theoretical study can be directly compared to experimental observations obtained for films grown by molecular beam epitaxy[24,26] (MBE) and pulsed-laser deposition (PLD).[27] In the work by Tober *et al.*,[24,26] MBE growth of epitaxial Fe-Ag and Co-Ag films on Mo(110) by both sequential and codeposition processes was observed to lead to the spontaneous formation of striped structures oriented along the Mo [100] direction (i.e., with composition modulation along the [10] direction in the notation of Secs. II and III) with periodicities on the order of 2–2.5 nm. Both the modulation direction and periodicity of the stripe structures

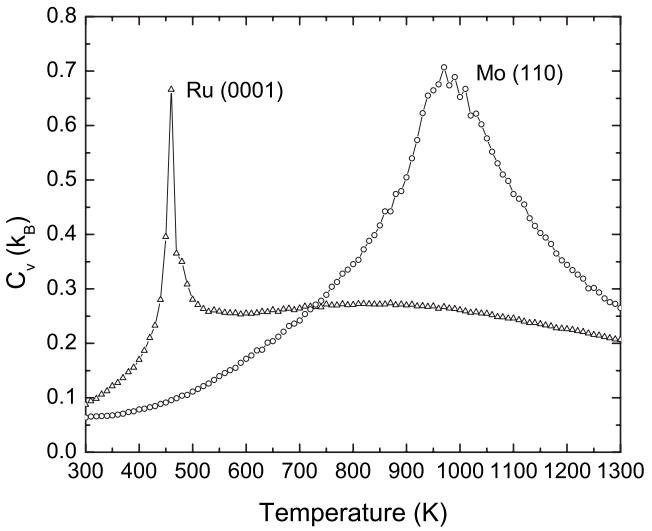

FIG. 10. Heat capacity (C_V) versus temperature at equal concentration for both the FeAg/Mo(110) and FeAg/Ru(0001) systems. The heat-capacity peak indicates the order-disorder phase transition.

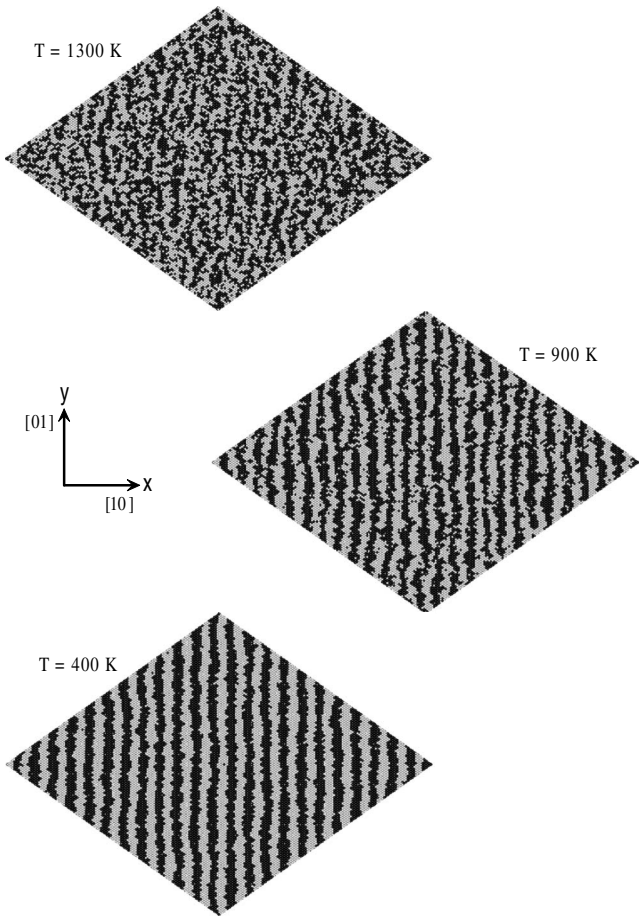

FIG. 11. Equilibrium snapshots for FeAg/Mo(110) system at 1300, 900, and 400 K.

observed by Tober *et al.*[24,26] are in excellent agreement with the predictions of the current study. In subsequent work by Borca *et al.*,[27] PLD growth of Fe-Ag films on Mo(110) was also observed to lead to the formation of stripe structures oriented along [100], although compared to the MBE results, the structures obtained by PLD are relatively more disordered and were reported to show slightly larger periodicities of approximately 3.5 nm. The better agreement of the present theoretical predictions for stripe periodicities with the results of Tober *et al.*[24,26] suggests that the slower growth conditions characteristic of MBE relative to PLD may lead to stripe periodicities corresponding more closely to the stable thermodynamic equilibrium structures in this system. For FeAg/Mo(110), a significant result of the present calculations concerns the relatively high thermal stability of the stripe structures, which are observed in MC simulations to remain ordered up to approximately 950 K. It is expected that the predicted order-disorder transition temperature cannot be directly verified by experiment due to the fact that such thin-film structures in ultrahigh vacuum will likely desorb at considerably lower temperatures. We note that in the work of Tober *et al.*,[24,26] it was stated that the stripe phases are stable up to $T \approx 250$ °C, although the structure of the films at higher temperatures was not described.

For FeAg/Ru(0001), we are not aware of published experimental data that can be directly compared to the predictions of the current study. However, the results obtained here are very similar to those derived in previous theoretical studies,[28,65] employing the same methodology for CoAg/Ru(0001) where comparisons can be made with previous experimental work. Both Co-Ag and Fe-Ag alloy systems feature similar size mismatch and both are bulk immiscible. Previous MC simulations for equiatomic CoAg/Ru(0001) (Ref. 65) yield results for the ordering transitions, stripe orientations, and periodicities that are nearly identical to those obtained in the present study for FeAg/Ru(0001). In contrast to FeAg/Ru(0001), detailed experimental investigations have been undertaken for CoAg/Ru(0001).[25,43] Unfortunately, direct comparisons between theoretical predictions and experimental measurements are complicated by the tendency of Ag films on Ru to form dislocated structures. Specifically, equiatomic monolayer films are observed to phase separate to a Co-rich alloy phase and a Ag-rich dislocated film upon annealing.[25] The composition modulation periodicities of a few nanometers predicted for CoAg and FeAg on Ru(0001) in this and previous[28] studies are, however, comparable to the characteristic length scales observed for disordered droplet patterns in pseudomorphic Co-rich alloys on Ru(0001).[43]

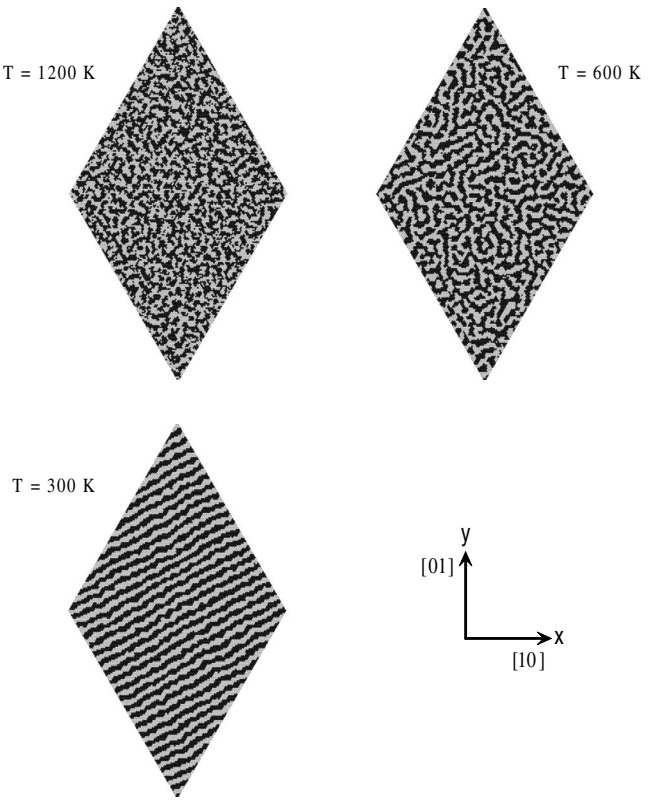

FIG. 12. Equilibrium snapshots for FeAg/Ru(0001) system at 1200, 600, and 300 K.

It is interesting to compare the results of the present MC calculations to previous investigations of stripe disordering phase transitions in dipolar lattice models. In general, the disordering behavior in such models is known to be influenced by the symmetry of the substrate (e.g., Ref. 66), which exerts a *p*-fold "symmetry breaking field," favoring stripe ordering along specific discrete directions. In recent Monte Carlo studies of two-dimensional dipolar systems on a

square lattice,[67] finite-size scaling analyses establish both continuous and first-order disordering transitions of stripe patterns; while we have not attempted detailed finite-size scaling analyses, the heat-capacity peaks and nature of the structural changes observed for the stripe-disordering transitions in the present simulations for FeAg on the twofold Mo(110) substrate are qualitatively similar with the second-order behavior observed in the square-lattice simulations for some values of the ratio of the strengths of the nearest-neighbor-exchange and dipolar interactions.

For FeAg/Ru(0001), our present results can be compared to the MC simulations carried out by Singer and co-workers[33–35] for a dipolar model on a sixfold symmetric triangular lattice. For systems with relatively small pattern periodicities, characterized by relatively large ratios of the strength of the nearest-neighbor to dipolar interactions (η as defined in Sec. II A), disordering of stripe and droplet patterns appears to occur via a continuous defect-induced melting transition of the KT type.[32,34,36–38] In the present work for FeAg/Ru(0001) and previous simulations[65] using the same underlying theory for the interactions in CoAg/Ru(0001), the Kosterlitz–Thouless character of the disordering transition has not been confirmed. Contrary to expectations of the KT theory, we find a pronounced peak in the heat capacity near the ordering transition. Although detailed finite-size scaling analyses would be required to make definitive conclusions about the exact nature of the disordering transitions in the FeAg/Ru(0001) and CoAg/Ru(0001) systems, a possible explanation for the discrepancy with the results obtained here with those for dipolar models may be associated with the exact nature of the interactions in epitaxial alloy films. We have shown above (cf. Fig. 9) that the elastic interactions on the length scale of the stripe patterns obey a decay law, which is not strictly dipolar in nature: Over intermediate ranges, they exponentially decay, eventually crossing over to the inverse cubic law at longer distances. Physically, this follows from the dominance of relaxations in the topmost surface layer over the substrate relaxation. A comparison of the present MC results and those obtained in previous simulations for dipolar lattice models suggests that the form of the interatomic pair interactions at intermediate ranges may affect the character of the ordering transition when the equilibrium stripe width has the same length scale as the exponential decay length of the interactions. While further work is clearly warranted to investigate this issue in detail, the present results suggest that modifications to standard statistical models of pattern formation may be required in applications to epitaxial alloys with periodicities on length scales of approximately ten atomic spacings.

VI. SUMMARY AND CONCLUSIONS

This paper has described details surrounding the application of the theoretical model of Ozoliņš *et al.*[28] in the first-principles modeling of nanoscale pattern-forming epitaxial alloy films. In Sec. II, the physical picture underlying the theoretical model was reviewed, and it was shown how the theory gives rise to three separate contributions to the effective-pair interactions underlying pattern formation in these systems: a short-ranged chemical contribution, a medium-ranged contribution originating from elastic displacements within the film layer, and a long-ranged dipolar contribution associated with substrate-mediated elastic displacements. The application of this theoretical model to alloy films on sixfold symmetric hexagonal (0001) and twofold symmetric bcc (110) surfaces was described in detail. Results for FeAg films on Ru(0001)and Mo(110) substrates were presented, and it was demonstrated that with four physically motivated parameters, the model is capable of accurately reproducing the energetics of both short-period stripe structures and the long-wavelength limiting behavior stemming from the differences in surface stress between Fe and Ag films on each substrate. In addition, for FeAg/Mo(110), where direct comparisons with experimental observations is possible, the model leads to a parameter-free prediction of the stable composition-modulation wavelength that is in excellent agreement with measurements for MBE-grown thin films in this system.

In applications of the theoretical formalism described in Sec. II to FeAg/Ru(0001), FeAg/Mo(110), and CoAg/Ru(0001) (Ref. 28) systems, the stable composition-modulation wavelengths are found to be governed by competition between the short-ranged chemical and medium-ranged elastically mediated contributions to the effective-pair interactions. The latter contributions are associated with displacements within the film layer and give rise to a contribution that is exponentially decaying in real space. These contributions are found to be dominant relative to the dipolar substrate-mediated interactions at length scales of a few nanometers. These results theoretically obtained for FeAg and CoAg films on Mo and Ru substrates are consistent with a very recent analysis of scanning-tunneling microscopy results for the oxygen on Pt(110) system,[44] where a (11×2) stripe superstructure is found to be stabilized by short-ranged elastic relaxations confined to the surface. Additionally, in previous work,[43] it was demonstrated that the Frenkel–Kontorova model, which assumes that elastic displacements are confined to within the alloy film, is capable of quantitatively reproducing displacement patterns measured by scanning-tunneling microscopy for nanometer-scale droplet structures in Co-rich CoAg epitaxial films on Ru(0001). The examples reviewed in this paragraph point to the inadequacy of traditional continuum models (see Sec. II B) for describing the energetics of compositionally patterned epitaxial structures at nanometer-scale wavelengths.

The results presented in this paper show how the theoretical model of Ref. 28 can be coupled with Monte Carlo simulations as a framework for investigating the finite-temperature stability of compositional patterns formed in a given alloy system. For FeAg films on Mo(110) and Ru(0001), stable stripe patterns are predicted at low temperatures on both substrates. In the former case, these are stable to very high temperatures, while in the latter case, the stripe structures are observed to be topologically disordered for temperatures above about 450 K. The much lower ordering temperature predicted for the Ru(0001) versus Mo(110) substrates is somewhat surprising considering that the depth of the interaction potential is actually larger in magnitude for the former system. This can be understood as a reflection of

the nearly isotropic nature of the ordering potential on the sixfold symmetric Ru(0001) substrate and the associated lower energy penalty associated with orientational disorder in the stripe patterns. The results of this study thus highlight the utility of employing anisotropic substrates for the purpose of stabilizing regular self-assembled compositional patterns.

ACKNOWLEDGMENTS

This research was supported by the National Science Foundation under Grants No. DMR-0502737 (B.Y. and M.A.) and No. DMR-0427638 (T.M. and V.O.). Research at UCLA (T.M. and V.O.) was also supported by the FCRP Center for Functional Engineered NanoArchitectonics (FENA).

*boyang@ucdavis.edu

[1] M. A. Kastner, Rev. Mod. Phys. **64**, 849 (1992).
[2] *Introducing Molecular Electronics*, edited by G. Cuniberti, G. Fagas, and K. Richter (Springer, Berlin, 2005).
[3] N. N. Ledentsov, V. M. Ustinov, V. A. Shchukin, P. S. Kop'ev, Z. I. Alferov, and D. Bimberg, Semiconductors **32**, 343 (1998).
[4] C. H. Bennett and D. P. D. Vincenzo, Nature (London) **404**, 247 (2000).
[5] V. A. Schukin and D. Bimberg, Rev. Mod. Phys. **71**, 1125 (1999).
[6] Ivan N. Stranski and L. Von Krastanow, Akad. Wiss. Lit. Mainz Abh. Math. Naturwiss. Kl. **146**, 797 (1939).
[7] M. Seul and D. Andelman, Nature (London) **267**, 476 (1995).
[8] D. J. Keller, H. M. McConnell, and V. T. Moy, J. Phys. Chem. **90**, 2311 (1986).
[9] M. Muthukumar, C. K. Ober, and E. L. Thomas, Science **277**, 1225 (1997).
[10] K. De'Bell, A. B. MacIsaac, and J. P. Whitehead, Rev. Mod. Phys. **72**, 225 (2000).
[11] S. A. Langer, R. E. Goldstein, and D. P. Jackson, Phys. Rev. A **46**, 4894 (1992).
[12] D. Vanderbilt, in *Computations for the Nano-Scale*, edited by P. E. Blöchl, A. J. Fisher, and C. Joachim (Kluwer, Dordrecht, 1993), p. 1.
[13] K. Thurmer, R. Q. Hwang, and N. C. Bartelt, Science **311**, 1272 (2006).
[14] R. Plass, J. A. Last, N. C. Bartelt, and G. L. Kellogg, Nature (London) **412**, 875 (2001).
[15] K. Pohl, M. C. Bartelt, J. de la Figuera, N. C. Bartelt, J. Hrbek, and R. Q. Hwang, Nature (London) **397**, 238 (1999).
[16] M. Batzill, F. Bardou, and K. J. Snowdon, Phys. Rev. Lett. **85**, 780 (2000).
[17] H. Chen, R. M. Feenstra, J. E. Northrup, T. Zywietz, and J. Neugebauer, Phys. Rev. Lett. **85**, 1902 (2000).
[18] J. B. Hannon, F.-J. Meyer zu Heringdorf, J. Tersoff, and R. M. Tromp, Phys. Rev. Lett. **86**, 4871 (2001).
[19] S. M. Driver and D. P. Woodruff, Surf. Sci. **492**, 11 (2001).
[20] B. Croset, Y. Girard, G. Prévot, M. Sotto, Y. Garreau, R. Pinchaux, and M. Sauvage-Simkin, Phys. Rev. Lett. **88**, 056103 (2002).
[21] R. Ragan, Y. Chen, D. A. A. Ohlberg, G. Medeiros-Ribeiro, and S. R. Williams, J. Cryst. Growth **251**, 657 (2003).
[22] M. Park, P. M. Chaikin, R. A. Register, and D. H. Adamson, Appl. Phys. Lett. **79**, 257 (2001).
[23] R. Q. Hwang, Phys. Rev. Lett. **76**, 4757 (1996).
[24] E. D. Tober, R. F. Farrow, R. F. Marks, G. Witte, K. Kalki, and D. D. Chambliss, Phys. Rev. Lett. **81**, 1897 (1998).
[25] G. E. Thayer, V. Ozoliņš, A. K. Schmid, N. C. Bartelt, M. Asta, J. J. Hoyt, S. Chiang, and R. Q. Hwang, Phys. Rev. Lett. **86**, 660 (2001).
[26] E. D. Tober, R. F. Marks, D. D. Chambliss, K. P. Roche, M. F. Toney, A. J. Kellock, and R. F. C. Farrow, Appl. Phys. Lett. **77**, 2728 (2000).
[27] B. Borca, O. Fruchart, and C. Meyer, J. Appl. Phys. **99**, 08Q514 (2006).
[28] V. Ozoliņš, M. Asta, and J. J. Hoyt, Phys. Rev. Lett. **88**, 096101 (2002).
[29] J. Tersoff, Phys. Rev. Lett. **74**, 434 (1995).
[30] V. I. Marchenko, JETP Lett. **33**, 381 (1981).
[31] K.-O. Ng and D. Vanderbilt, Phys. Rev. B **52**, 2177 (1995).
[32] M. M. Hurley and S. J. Singer, Phys. Rev. B **46**, 5783 (1992).
[33] A. D. Stoycheva and S. J. Singer, Phys. Rev. Lett. **84**, 4657 (2000).
[34] A. D. Stoycheva and S. J. Singer, Phys. Rev. E **64**, 016118 (2001).
[35] A. D. Stoycheva and S. J. Singer, Phys. Rev. E **65**, 036706 (2002).
[36] J. Villain and P. Bak, J. Phys. (Paris) **42**, 657 (1981).
[37] D. A. Huse and M. E. Fisher, Phys. Rev. B **29**, 239 (1984).
[38] K. J. Strandburg, Rev. Mod. Phys. **60**, 161 (1988).
[39] A. B. Kashuba and V. L. Pokrovsky, Phys. Rev. B **48**, 10335 (1993).
[40] F. C. Frank and J. H. van der Merwe, Proc. R. Soc. London **198**, 205 (1949).
[41] D. Vanderbilt, O. L. Alerhand, R. D. Meade, and J. D. Joannopoulos, J. Vac. Sci. Technol. B **17**, 1013 (1989).
[42] D. Vanderbilt, Surf. Sci. **268**, L300 (1992).
[43] G. E. Thayer, N. C. Bartelt, V. Ozoliņš, A. K. Schmid, S. Chiang, and R. Q. Hwang, Phys. Rev. Lett. **89**, 036101 (2002).
[44] S. Helveg, W. X. Li, N. C. Bartelt, S. Horch, E. Lægsgaard, B. Hammer, and F. Besenbacher, Phys. Rev. Lett. **98**, 115501 (2007).
[45] B. Sadigh, M. Asta, V. Ozoliņš, A. K. Schmid, N. C. Bartelt, A. A. Quong, and R. Q. Hwang, Phys. Rev. Lett. **83**, 1379 (1999).
[46] B. D. Krack, V. Ozoliņš, M. Asta, and I. Daruka, Phys. Rev. Lett. **88**, 186101 (2002).
[47] B. Yang, Ph.D. thesis, Northwestern University, 2006.
[48] M. A. Krivoglaz, *X-Ray and Neutron Diffraction in Nonideal Crystals* (Springer, Berlin, 1996).
[49] L. D. Landau and E. M. Lifshitz, *Theory of Elasticity* (Pergamon, Oxford, 1986).
[50] A. N. Stroh, Philos. Mag. **3**, 625 (1958).
[51] T. C. T. Ting, Q. J. Mech. Appl. Math. **45**, 119 (1992).
[52] L. E. Shilkrot and D. J. Srolovitz, Phys. Rev. B **53**, 11120 (1996).
[53] D. Vanderbilt, Phys. Rev. B **41**, 7892 (1990).

[54] G. Kresse and J. Fürthmuller, Phys. Rev. B **54**, 11169 (1996).
[55] G. Kresse and J. Fürthmuller, Comput. Mater. Sci. **6**, 15 (1996).
[56] J. P. Perdew, J. A. Chevary, S. H. Vosko, K. A. Jackson, M. R. Pederson, D. J. Singh, and C. Fiolhais, Phys. Rev. B **46**, 6671 (1992).
[57] M. J. Mehl, B. M. Klein, and D. A. Papaconstantopoulos, *Intermetallic Compounds* (Wiley, New York, 1994), Vol. 1, Chap. 9.
[58] K. W. Katahara, M. H. Manghnani, and E. S. Fisher, J. Phys. F: Met. Phys. **9**, 773 (1979).
[59] G. Simmons and H. Wang, *Single Crystal Elastic Constants and Calculated Aggregate Properties: A Handbook* (MIT, Cambridge, 1971).
[60] P. E. Blöchl, Phys. Rev. B **50**, 17953 (1994).
[61] G. Kresse and D. Joubert, Phys. Rev. B **59**, 1758 (1999).
[62] J. A. Nelder and R. Mead, Comput. J. **7**, 308 (1965).
[63] Z. W. Lu, D. B. Laks, S. H. Wei, and A. Zunger, Phys. Rev. B **50**, 6642 (1994).
[64] H. Okamoto, P. Subramanian, and L. Kacprzak, *Binary Alloy Phase Diagrams*, 2nd ed. (ASM International, Metals Park, OH, 1996).
[65] V. Ozoliņš (unpublished).
[66] J. V. José, L. P. Kadanoff, S. Kirkpatrick, and D. R. Nelson, Phys. Rev. B **16**, 1217 (1977).
[67] E. Rastelli, S. Regina, and A. Tassi, Phys. Rev. B **73**, 144418 (2006).